fibers

MDPI

Article

Conversion of Animal-Derived Protein By-Products into a New Dual-Layer Nanofiber Biomaterial by Electrospinning Process

Carmen Gaidău [1], Maria Râpă [2,*], Laura Mihaela Stefan [3], Ecaterina Matei [2], Andrei Constantin Berbecaru [2,*], Cristian Predescu [2] and Liliana Mititelu-Tartau [4]

[1] The National Research & Development Institute for Textiles and Leather-Division Leather and Footwear Research Institute, 031251 Bucharest, Romania; carmen_gaidau@hotmail.com
[2] Faculty of Material Science and Engineering, National University of Science and Technology Politehnica Bucharest, 060042 Bucharest, Romania; ecaterina.matei@upb.ro (E.M.); cristian.predescu@upb.ro (C.P.)
[3] Department of Cellular and Molecular Biology, National Institute of Research and Development for Biological Sciences, 296 Splaiul Independenței, Sector 6, 060031 Bucharest, Romania; lauramihaelastefan@yahoo.com
[4] Pharmacology, Clinical Pharmacology and Algesiology Department, Faculty of Medicine "Grigore T. Popa", University of Medicine and Pharmacy, 700115 Iasi, Romania; liliana.tartau@umfiasi.ro
* Correspondence: maria.rapa@upb.ro (M.R.); andrei.berbecaru@upb.ro (A.C.B.)

Abstract: The aim of this study was to design a dual-layer wound dressing as a new fibrous biomaterial based on the valorization of animal-derived proteins. The first layer was fabricated by the deposition of poly(ethylene oxide) (PEO) loaded with keratin hydrolysate (KH) via a mono-electrospinning process onto a poly(lactic acid) (PLA) film, which was used as a support. The second layer consisted of encapsulating a bovine collagen hydrolysate (CH) into poly(vinyl pyrrolidone) (PVP) through a coaxial electrospinning process, which was added onto the previous layer. This assemblage was characterized by electronic microscopy for morphology and the controlled release of KH. In vitro biocompatibility was evaluated on the L929 (NCTC) murine fibroblasts using quantitative MTT assay and qualitative cell morphological examination after Giemsa staining. Additionally, in vivo biocompatibility methods were used to assess the impact of the biomaterial on white Swiss mice, including the evaluation of hematological, biochemical, and immunological profiles, as well as its impact on oxidative stress. The results revealed a nanofibrous structure for each layer, and the assembled product demonstrated antioxidant activity, controlled release of KH, a high degree of in vitro biocompatibility, negligible hematological and biochemical changes, and minimal impact of certain specific oxidative stress parameters compared to the use of patches with textile support.

Keywords: collagen hydrolysate; keratin hydrolysate; biomaterial; nanofibers; electrospinning; wound dressing

Citation: Gaidău, C.; Râpă, M.; Stefan, L.M.; Matei, E.; Berbecaru, A.C.; Predescu, C.; Mititelu-Tartau, L. Conversion of Animal-Derived Protein By-Products into a New Dual-Layer Nanofiber Biomaterial by Electrospinning Process. *Fibers* **2023**, *11*, 87. https://doi.org/10.3390/fib11100087

Academic Editor: Marija Gizdavic-Nikolaidis

Received: 31 August 2023
Revised: 25 September 2023
Accepted: 11 October 2023
Published: 14 October 2023

1. Introduction

In accordance with the Food and Agriculture Organization (FAO)'s latest statistical yearbook, the livestock population in 2021 was estimated to be around 4.89 billion, which includes bovine (1.5 billion), goat (1 billion), ovine (1.3 billion), and swine (1.1 billion) animals [1]. A considerable quantity of proteins is derived from the processing of mammal skins (cattle, sheep, etc.) and sheep's wool, which can be exploited due to their bioactive potential for the regeneration of damaged human tissues. The meat industry also generates an important quantity of collagen and gelatin as by-products from the tendons and hides of slaughtered cattle [2]. These proteins can be exploited to create cosmetic skin-care preparations [2], fabrication of various biomaterials for the biomedical field such as wound dressings in the form of sponges [3], small pellets for drug delivery [4], nanoparticles for gene delivery [5], protective shields employed in ophthalmology [6], and biomaterials to assist in the development of neo-organs [7]. Due to advancements in animal production practices, livestock waste and by-products can now be repurposed and treated to

yield fertilizers [8–10], feed [11,12], and biopolymers [13–16], resulting in a substantial reduction of pollution. Nonetheless, the development of biomaterials could present a more effective approach to managing animal by-products, as it can generate innovative biomedicals for pharmaceutical applications [17]. For example, sheep teeth dentine-derived hydroxyapatite (HA) served as an alternative bioactive biomaterial source for fabricating scaffolds employed to stimulate the growth of bone and tissue and the proliferation of fibroblast cells [17]. In other studies, the biocompatible ceramic, HA, was extracted from bovine bones [18,19] and utilized in a range of biomedical applications [20,21]. One advantage of bio-ceramic materials made from naturally sourced biological apatites is their cost-effectiveness.

Collagen and keratin are two important proteins found in the extracellular matrices (ECM) of tissues and organs, and they play crucial roles in providing structural support and maintaining the integrity of various biological structures. Collagen, found abundantly in mammals, functions as a primary component in skin, blood vessels, bones, tendons, and heart tissue. It has been effectively employed in both in vitro and in vivo tissue regeneration and engineering applications [22]. Collagen is well-known for accelerating the formation of fibroblasts and the closure of wounds. It was reported that the collagen rabbit glue derived from the skins of rabbits was processed into nanofibers [23], leading to an increase in its surface area and improvement in the mechanical properties, making it an ideal scaffold material for promoting cell growth and tissue regenerations. Using a water-based dispersant containing titanium dioxide nanoparticles (TiO_2 NPs) in the anatase form, combined with nitrogen and silver nanoparticles, along with the use of chitosan with a high molecular weight, excellent biocompatibility and antimicrobial properties were achieved. These characteristics make collagen a highly promising material for tissue engineering applications [24]. Collagen nanofibers are considered ideal for supporting cell proliferation and tissue regeneration.

Keratin is a type of polypeptide molecule made up of multiple amino acids that contain both inter-molecular bonds formed by disulfide-cysteine amino acids and intra/inter-molecular bonds of polar and non-polar amino acids [25]. It is both water-insoluble and resistant to a variety of weak alkalis, acidic solutions, and organic solvents. Additionally, keratin exhibits resistance against protein-digesting enzymes such as trypsin and pepsin [26]. Keratin promotes cell adhesion, proliferation, and migration due to the presence of Arg-Gly-Asp and Leu-Asp-Val tripeptides. Keratin, in particular, demonstrates an increased stability due to the cysteine disulfide cross-links that form within and between protein chains [27]. The presence of keratin as a constituent provides exceptional characteristics that make it a highly effective biomaterial. Nevertheless, the absence of standardized protocols for biomaterial preparation, particularly regarding pre-treatment, extraction, chemical modifications, and purification, hinders its ongoing commercial production. Keratin is used in wound dressing materials because it helps maintain their integrity in the epithelium. Furthermore, keratin exhibits antioxidant and antimicrobial properties due to the presence of S-sulfonated cysteine groups in soluble keratin extracts [28]. Utilizing animal-derived proteins in wound dressings through the electrospinning process, in contrast to synthetic polymers and cotton knitted textiles, represents an eco-friendly method because it involves the use of non-toxic solvents in solution preparation and, furthermore, these proteins exhibit antimicrobial and biocompatible attributes [23,29].

Electrospinning employs an electric field to pull a polymer solution or molten material into a fine fiber. The process typically requires the preparation of an animal-derived protein extract, loading it into a syringe, and applying an electric field to the solution, inducing the solution to create a fine fiber, which is collected on a grounded surface. The nanofibers possess a high surface area-to-volume ratio, which enhances their capacity to facilitate cell adhesion and growth. Also, the nanofibers can be functionalized with bioactive molecules such as growth factors or peptides to further enhance their regenerative properties. The recent advances in electrospinning-based advanced wound dressings show a novel approach of utilizing a sequence of pin-ring-structured collectors as a means to collect electrospun

nanofibers [30]. This novel approach enhances both the water-attracting properties and mechanical characteristics of electrospun nanofibers when compared to the traditional, randomly arranged nanofiber structure. Furthermore, the radially arranged nanofiber pattern has been shown to significantly facilitate alignment, enhance adhesion, and promote cell proliferation in comparison to the randomly oriented nanofiber group [30]. Another paper reported porous nanofiber membranes obtained by electrospinning as innovative materials for enhancing wound healing [31]. These membranes have the potential to enhance protein attachment, stimulate cell adhesion, and facilitate diffusion and cell growth. Through the incorporation of various biopolymers and antimicrobial agents, adjustments in water transport, and achieving a high swelling rate, these membranes exhibit a high tensile strength. Additionally, they exhibit notable in vitro coagulation capabilities and demonstrate enhanced antimicrobial properties against both Staphylococcus aureus and Escherichia coli [31].

However, a significant number of current wound healing materials rely on single-layer nanofibers and do not fully satisfy the criteria for ideal wound healing. In this study, dual nanofiber layers based on polymeric matrices such as poly(lactic acid) (PLA), poly(ethylene oxide) (PEO), and poly(vinyl pyrrolidone) (PVP) were created by using mono- and coaxial electrospinning technology for potential wound dressing applications. These polymeric matrices were loaded with keratin (KH) and bovine collagen hydrolysates (CH), respectively, which are biodegradable natural polymers that are highly applicable in tissue engineering due to their lower costs. Two-layer structures were used to incorporate different materials in each layer: PLA, PEO, and KH in the first layer, and PVP and CH in the second layer. The first layer provides protection and prevents external contamination, as well as serves as a barrier that prevents excessive moisture loss from the wound. At the same time, KH is released in a controlled manner through the second layer and arrives at the wound. The second layer was designed for wound exudate management, to maintain a moist wound environment, and to heal the wound due to the CH delivery. This dual functionality improves the overall wound healing. The two-layer structure will be easier to apply without the necessity to remove the dressing, so the frequency of dressing changes will be reduced. The advantages of creating nanofibers in this way consist in ensuring good mechanical strength, biocompatibility of dressings and avoidance of bacteria attaching due to the PLA [32], and the controlled release of bioactive proteins derived from animals due to the PEO and PVP matrices, leading to the healing of wound as well as the ability to keep the dressing on throughout the healing process. This assembled structure (PLA/PEO/KH—first layer, PVP/CH—second layer) may offer other benefits due to the addition of CH and KH, such as the antioxidant activity of the biomaterial, which could have potential benefits for skin health and the valorization of animal by-products. Electron microscopy and spectrophotometric assays were used to examine the morphology and in vitro biocompatibility of the electrospun nanofibers. In vivo tests were performed to analyze various parameters, such as leukocyte count, liver enzymes, and immunological responses, to assess the impact of different batches of nanofibers on the health and immune system of the animals.

2. Materials and Methods

2.1. Materials

A degradable and environmentally friendly PLA, NatureWorks® Ingeo™, 4032D grade (Minnetonka, MN, USA); PEO as power shape (MW 100,000, Alfa Aesar, Kandel, Germany); and a synthetic polymer PVP, K90 for molecular biology, MW = 100,000–150,000 g/mol (PanReac AppliChem, Darmstat, Germany), which exhibit good low chemical toxicity and adhesion properties [33], were used as polymeric matrices. Dichloromethane (DCM), dimethylformamide (DMF), and ethanol, all of analytical grade, were used as solvents. Other chemicals of analytical grade were used.

Collagen hydrolysate (CH) and keratin hydrolysate (KH) were extracted from indigenous by-products obtained from the leather industry.

Figure 1 shows the chemical structures of polymers used in this study.

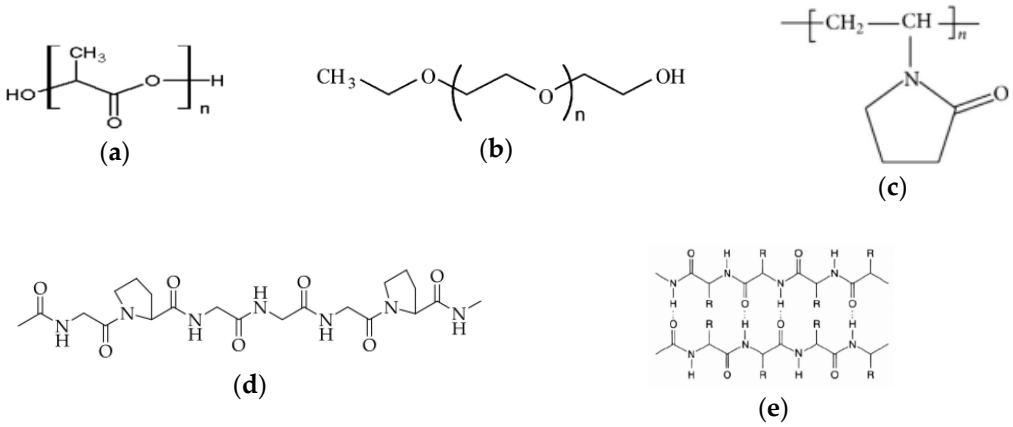

Figure 1. Chemical structure for: (**a**) PLA [34], (**b**) PEO (reprinted with permission from [35]. Copyright 2023 American Chemical Society), (**c**) PVP [36], (**d**) CH [37], and (**e**) Beta-Keratin [38].

Table 1 displays the physico-chemical characteristics of concentrated CH and KH utilized in this research.

Table 1. Physico-chemical properties of concentrated collagen and keratin hydrolysates.

Property	Mean Value ± Standard Deviation	
	***Collagen Hydrolysate* (*CH*)**	***Keratin Hydrolysate* (*KH*)**
Dry matter (%)	60.40 ± 0.42	9.00 ± 0.05
Ash (%)	6.24 ± 0.27	13.68 ± 0.25
Total nitrogen (%)	14.67 ± 0.66	14.20 ± 0.57
Protein (%)	82.43 ± 2.66	80.65 ± 1.40
pH (pH units)	8.54 ± 0.10	11.85 ± 0.09
Aminic nitrogen (%)	1.43 ± 0.06	1.34 ± 0.06
Electrical conductivity (µs/cm)	870 ± 0.1	13,700 ± 20

2.2. Extraction of KH and CH Derived from Animal By-Products

The extraction of hydrolyzed collagen (CH) from discarded bovine leather was carried out by using 10% (*w*/*v*) calcium hydroxide and 1% (*w*/*v*) Alcalase 2.4 L (Novozymes) at temperatures of 80 °C and 60 °C, respectively [39]. The obtained collagen was then concentrated to around 60% (*w*/*w*) at a temperature of 60 °C using a Hei-VAP Rotary Evaporator (Schwabach, Germany). This concentration step led to an increase in the viscosity of the collagen hydrolysate, rendering it suitable for spinning. To eliminate any remaining traces of chromium, several intermediary steps were carried out, including filtration through media having a pore size dimension of 0.45 µm and decantation after both the alkaline and enzymatic hydrolysis phases.

Initially, the wool from the sheepskin underwent degreasing by employing a solution consisting of 1% surfactant, 1% sodium carbonate (Na_2CO_3), and 2% ammonium hydroxide (NH_4OH) with a concentration of 24%, all conducted at a temperature of 50 °C for 2 h. Subsequently, the keratin within the material was dissolved using a 2.5% (*w*/*v*) sodium hydroxide (NaOH) solution known as rotulis (Lach-Ner sro) at 80 °C for 4 h. The resulting keratin hydrolysate (KH) was then separated by decanting, followed by filtration, centrifugation, and ultimately freeze-drying [40].

2.3. Preparation of Electrospinning Solutions

A 10% (*w*/*v*) PLA solution was prepared by dissolving it in a blend of DCM and DMF solvents (7:3 vol%) under magnetic stirring at 60 °C for 6 h and a speed of 400 rpm. Subsequently, PEO, in powdered form, was introduced into the PLA solution to achieve a total polymer content of 12.5 w%. Then, 1% KH was added to the PLA/PEO mixture by continuous stirring until complete homogenization.

For the preparation of a 10% PVP solution in ethanol, the PVP was dissolved using magnetic stirring at room temperature until complete dissolution was achieved.

To prepare a 10% (*w*/*v*) solution of CH, the CH underwent dissolution in a 9:1 (*v*/*v*) mixture of acetic acid in distilled water.

2.4. Fabrication of the Dual-Layer Nanofiber Biomaterial

An Electrospinning machine designed as TL-Pro-BM (Tong Li Tech Co., Ltd., Bao An, Shenzhen, China) was used for the fabrication of the dual-layer biomaterial. The machine comprises a syringe pump, a high-voltage power supplier, and a grounded conductive drum collector. The principle of electrospinning involves using an electric field to draw a charged polymer solution from a spinneret (a small nozzle) to a grounded or oppositely charged collector plate. A high voltage applied to the spinneret creates a strong electric field between the spinneret and the collector that causes the polymer jet to be continuously pulled and stretched toward the collector [41]. The electrostatic repulsion between these charges overcomes the surface tension of the polymer solution, leading to the formation of thinner and more uniform fibers.

The first layer consisting of PLA/PEO/KH nanofibers was fabricated via a monoaxial electrospinning technique and served as a collected support for the next layer. Preliminary experiments were conducted using various electrospinning parameters for optimizing the PLA and PLA/PEO nanofibers production. The production of uniform fibers without visible beads was observed. This consisted in varying the concentration of the PLA solution from 8 wt.% to 12 wt.%, negative voltage from −15.22 kV to −9.01 kV, flow rate from 5 mL/h to 2 mL/h, as well as the distance between the needle to collector from 15 cm to 13 cm. Then, when the SEM images showed a good appearance, the experiment continued with the introduction of KH. The second layer consisted of the encapsulation of the CH solution into a PVP solution via coaxial electrospinning using two concentrically arranged nozzles with G15 and G21 dimensions. To gain a deeper insight into the impact of KH and CH on the morphology and biological properties of prepared biomaterial, a PLA/PEO/PVP layer was also electrospun (first, the PLA/PEO solution was processed; then, the PVP solution was deposited onto PLA/PEO nanofibers). Each solution containing the protein, polymer, and solvent was introduced into a 10 mL Teflon syringe and passed through a metal needle connected to the end of the tubing. The resulting electrospun nanofibers were gathered on a drum that had been coated with aluminum foil.

Preparation parameters play a crucial role in shaping the characteristics of electrospun nanofibers, making them indispensable for achieving the desired outcomes. These parameters encompass three key categories that impact the nanofibers' morphology and mechanical properties: (i) process parameters, (ii) polymer solution parameters, and (iii) environmental conditions. Process parameters encompass factors such as voltage, liquid advancing speed, and the distance between the capillary needle and collector. The composition of nanofibers produced during the experiments and the technical parameters used for the electrospinning process are listed in Table 2. The collection of individual nanofibers took place over 180 min, while the assembly of the biomaterial required 90 min for PLA/PEO/KH and PVP/CH layers. The trials were conducted within a temperature range of 23 ± 1.1 °C and a relative humidity level of 36 ± 3.5%.

Table 2. Compositions and optimal conditions for producing the dual-layer nanofiber biomaterial through electrospinning.

Composition	Electrospinning	Flow Rate (mL/h)	Voltage (kV)	Distance between Needle and Collector (cm)	Collection Time (min)
PLA/PEO	Monoaxial	2.8	22.79	13	180
PLA/PEO/KH	1st layer, monoaxial	5.7	22.96	13	180
PLA/PEO/PVP	Monoaxial	4.0	19.29	13	180
PVP/CH	2nd layer, coaxial	3.5; 2.5	21.10	13	180
PLA/PEO/KH-PVP-CH	Assembled structure				90-90

Wound dressings should meet various criteria, including mechanical properties, biocompatibility, moisture management, antimicrobial properties, as well as ease of application and removal, when selecting the most suitable dressing for a specific wound type. PLA is an important bioresorbable polymer used in the development of wound dressings due to its excellent biocompatibility and biodegradability characteristics [42]. It naturally gets absorbed by the body and serves as a carrier for the controlled release of bioactive compounds. However, pure PLA lacks hydrophilicity, mechanical properties, and bioactivity, which significantly limits its applications in wound healing management. In other studies, wound dressings fabricated through an electrospinning process incorporated graphene oxide (GO) into a PLA solution at concentrations of up to 1% to enhance hydrophilicity or used quercetin (Q) to enable rapid and complete release under external electrical stimulation within just 1–2 min [43]. Some compositions included 1% CuO and ZnO NPs/2% tranexamic acid (TXA) to improve hydrophilicity [44] or 1% babassu oil to maintain a humid environment around the wound [45]. The reported tensile strength of human skin falls within the range of 1 to 40 Mpa. The aloin/PVP-Aloin/PVP/PLA-PLA sandwich nanofiber wound dressings were engineered to have tensile strengths within this range [46].

2.5. Investigation Methods

2.5.1. Morphology Examination

The FEI Quanta 450 FEG (Field Emission Gun) Scanning Electron Microscope (SEM) (Eindhoven, The Netherlands) was used in conjunction with a Secondary Electron Detector to generate high-resolution images of the samples. Energy Dispersive X-Ray (EDS) Spectrometry was used to analyze the elemental composition of samples at an accelerated voltage of 30 kV. The morphology and composition of the PLA/PEO, PLA/PEO/KH, PLA/PEO/PVP, and PLA/PEO/KH-PVP/CH nanofibers were investigated. To mitigate charging effects during SEM imaging, the electrospun nanofiber samples were deposited on a copper band, as a conductive substrate, and coated with a conductive layer of Au measuring approximately 5 nm in thickness.

2.5.2. Attenuated Total Reflectance Fourier Transform Infrared Spectroscopy (ATR FT-IR)

The INTERSPEC 200-X spectrophotometer (Interspectrum, Tartumaa, Estonia) was employed to determine the chemical composition of PLA/PEO/PVP and PLA/PEO/KH-PV/CH electrospun nanofibers. The spectra were taken in the absorption mode at a wavenumber ranging from 4000 to 750 cm^{-1} at a resolution of 4 cm^{-1}.

2.5.3. ABTS Free Radical Scavenging Assay

An improved ABTS discoloring assay was employed for the biomaterial analysis, wherein the 2,2′-azino-bis-(3-ethylbenzothiazoline-6-sulfonate) radical cation (ABTS+•) was generated by reacting a 7 mM stock solution of ABTS in the presence of 2.45 mM potassium persulphate. The resulting blend was allowed to stand in darkness for at least 16 h at room temperature prior to utilization. Afterward, the ABTS+• solution was diluted until it reached an absorbance of 0.7 ± 0.05 at 750 nm. Subsequently, a certain amount of biomaterial nanofibers was combined with 4 mL of the ABTS+• solution and maintained in darkness at room temperature for 15 min. The capability of the proteins to quench ABTS free radicals was evaluated using Equation (1):

$$\text{ABTS Free Radical Scavenging Activity } (\%) = \frac{(A_c - A_s)}{A_c} \times 100 \quad (1)$$

The absorbance of the control and sample is denoted as A_c and A_s, respectively. The antioxidant activity was subjected to three replicates (n = 3), and the reported value is the mean average with the corresponding standard deviation (S.D.).

2.5.4. Controlled Release of KH

The release of KH from the PLA/PEO/KH-PVP/CH nanofibers was assessed by employing UV-Vis spectroscopy with the aid of a UV-Vis spectrophotometer. The pre-established KH specific calibration curve (0–2000 ppm) was derived. The PLA/PEO/KH-PVP/CH nanofibers and PLA/PEO as control were immersed into distilled water and mixed at room temperature for 60 min. The absorbance of the supernatant was monitored at a wavelength of 285 nm using a quartz cell with a path width of 1 cm. The estimation of the cumulative release of KH was determined in accordance with Equation (2):

$$\text{Cumulative Release (\%)} = \text{Total protein released over time/Initial protein concentration (\%)} \quad (2)$$

2.5.5. In Vitro Cytocompatibility Testing

The direct contact method and NCTC clone L929 mouse fibroblasts (European Collection of Authenticated Cell Cultures—ECACC) were used to test the cytocompatibility of the nanofibers. Biomaterial samples measuring 5 × 5 mm were prepared and sterilized under UV light for a duration of 4 h. NCTC mouse fibroblasts were maintained in a minimum essential medium (MEM) supplemented with 10% fetal bovine serum (FBS) and a 1% mix of antibiotics (penicillin, streptomycin, and neomycin) and, then, seeded in 24-well culture plates at a density of 5×10^4 cells/mL. After 24 h of cell incubation at 37 °C, in a humidified atmosphere containing 5% CO_2, the culture medium was replaced with fresh mediu, and one nanofiber sample was added into each well. The nanofiber samples were added into the plates as 1 disk per well. The cells were then incubated further under standard conditions for both 24 h and 72 h, respectively. The control was represented by untreated cells.

The 3-(4,5-dimethylthiazol-2-yl)-2,5-diphenyltetrazolium bromide (MTT) assay was used to evaluate cell viability. This assay is based on the capacity of viable cells' mitochondrial succinate dehydrogenases to convert MTT into insoluble purple formazan crystals. The culture medium was substituted with a 0.25 mg/mL MTT solution, and the cells were allowed to incubate at 37 °C for 3 h. Subsequently, the insoluble formazan crystals were dissolved using isopropanol, gently stirring for 15 min at room temperature, and the absorbance was recorded at 570 nm with a SPECTROstar® Nano microplate reader (BMG, Berlin, Germany). The amount of converted dye was directly correlated with the number of metabolically active cells. The results were expressed as the percentage of cell viability relative to the control, which was considered to have 100% viability. Data were shown as the average of three measurements with the corresponding standard deviation (S.D.).

Additionally, cell morphology was assessed after 72 h of cell incubation in the presence of the nanofiber samples using Giemsa staining. Light microscope images of NCTC fibroblasts were acquired using a Zeiss Axio Observer D1 light microscope and subjected to analysis using AxioVision 4.6 software (Carl Zeiss, Oberkochen, Germany).

2.5.6. In Vivo Biocompatibility Testing

For the experimental research, white Swiss mice that were healthy adults (3 months old) and weighed between 25 and 30 g were used and were purchased from the Cantacuzino Institute in Bucharest, Băneasa Resort. They had a uniform gender distribution and were not genetically modified. The mice were obtained for use at the "Grigore T. Popa" University of Medicine and Pharmacy in Iasi. The animals were introduced to the laboratory setting a week prior to the experiments for acclimatization to standard environmental conditions, which included a steady temperature of 21 °C ± 2 °C, relative humidity ranging from 50% to 70%, and a lighting schedule of 12 h of light followed by 12 h of darkness. During this acclimatization period, they were housed individually in cages and had access to pellet-type granulated food and water without restriction. To prevent the effects of chronobiological factors, the experiments were conducted between 8 a.m. and 12 a.m. daily. The research protocol was drawn up, and the University's Ethics Commission's Approval (No. 5105/7.03.2022) was obtained, in accordance with international ethical standards regarding animal studies.

Test nanofibers packaged in blister paper deposited on the adhesive support were used according to the following codes: witness, PLA/PEO, PLA/PEO/KH, PLA/PEO/PVP, PVP/CH, and PLA/PEO/KH-PVP/CH.

The animals were sorted into six groups of five mice each in a random manner. On the first day of the experiment, the mice were subjected to anesthetisia through an intraperitoneal injection containing a mixture of 50 mg/kg Ketamine and 10 mg/kg Xylazine. The integuments on the left dorsal area were carefully shaved, and a small incision measuring 0.5 cm in length was created, running parallel to the spine. The nanofiber-impregnated sheet (dimensions 0.8 cm/0.8 cm) was placed onto a sterile textile material found on a commercial patch. It was then applied over the incision site, securely adhering to the skin with the help of the adhesive system. For the control group, the mice received an identical treatment using a standard patch featuring the same sterile textile material.

After making the skin incision and covering it with the test devices, the animals' conditions were continuously observed, including monitoring their respiration, spontaneous motility, motor coordination, food and water intake, stereotyped actions, and personal hygiene. On the 7^{th} day, the patches were removed, and the area around the incision was macroscopically inspected to detect any local tissue alterations.

The In vivo evaluation of the nanofiber biocompatibility involved studying the influence of their use on some hematological, biochemical, and immunological constants, as well as oxidative processes.

At 24 h and 7 days after the application of simple or nanofiber patches, the mice were subjected to anesthesia using 1% isoflurane. Blood samples were obtained from the lateral vein of their tail for the determination of various parameters including blood count, glutamic-pyruvic transaminase (TGP), glutamic-oxalacetic transaminase (TGO), lactate dehydrogenase (LDH), urea, and creatinine [47,48]. The tail of the animals was immersed in warm water at a temperature of 40 °C to expand the lateral vein. The tail was maintained in an extended position, and the lateral caudal vein was located at a distance of 3 cm from the tip. This specific area was antisepticised with a 70% alcohol solution [49–51]. Under local anesthesia achieved using 1% benzocaine spray, the vein was punctured, and 0.3 mL of blood was extracted [52].

To perform the blood count, the blood samples were gathered in vacutainers that included EDTA as an anticoagulant. The determinations were made using the automatic analyzer HEMAVET 950 (Oxford, UK), which operates based on flow cytometry with fluorescence. For biochemical assessments, venous blood collected on heparin and the ACCENT 200 biochemistry analyzer (Cormay, Warsaw, Poland) were employed.

To study the influence of nanofibers on oxidative processes, the activity of superoxide dismutase (SOD) and glutathione peroxidase (GPx) was monitored. SOD activity in the blood was determined using the colorimetric technique utilizing xanthine and xanthine oxidase and making use of RANSOD kits provided by RANDOX Laboratories Ltd. (Warsaw, Poland). This assessment was conducted on blood samples of a 0.3 m volume that had been obtained using heparin. Serum GPx values were measured from 0.3 mL blood collected on heparin, and the enzyme's activity was assessed through an enzymatic method employing the RANSEL kit from RANDOX Laboratories Ltd. (Warsaw, Poland).

Following a 7-day experiment, serum opsonic capacity (CO) was assessed using *Staphylococcus aureus* 94 cultures. The animals were then euthanized under general anesthesia using 2% isoflurane [51]. Peritoneal macrophages were collected from the intact peritoneal cavity through a 10 mL of HANKS solution rinse at 37 °C, followed by centrifugation at 1000 rotations per minute for 10 min. Subsequently, they were subjected to a 48 h incubation with *Staphylococcus aureus* 94 cultures at 37 °C to assess their phagocytic capacity (CF) and the bactericidal capacity (CB) of peritoneal macrophages by reseeding the samples on the culture media [53].

Euthanasia was carried out in a manner that ensured the animals experienced no physical or mental distress, resulting in rapid unconsciousness, the cessation of heart and respiratory functions, ultimately leading to their eventual death. This standard pro-

cedure was carried out in dedicated necropsy rooms separate from the animals' living quarters [54,55].

2.5.7. Statistical Analysis

The results were presented as the average value with the standard deviation (S.D.) for each specific parameter and substance examined individually. Statistical assessment was carried out through the unifactorial ANOVA approach utilizing the SPSS software, version 17.0 for Windows 10. The probability coefficient (p) being below 0.05 was considered as having statistical significance.

3. Results

3.1. SEM Morphology

SEM images revealed a surface that was both smooth and uniform in its appearance, without crack, pore, and bead for PLA/PEO nanofibers (Figure 2a). It was found that the mean size of the nanofibers was 523 ± 175 nm for PLA/PEO, 523 ± 175 nm for PLA/PEO, 375 ± 95 nm for PVP/CH, 872 ± 645 nm for PLA/PEO/KH, and 378 ± 102 nm for PLA/PEO/PVP. The introduction of KH into the PLA/PEO solution led to the creation of many beads (Figure 2b). The high viscosity of KH is the reason behind this. Numerous studies have indicated that boosting solution viscosity, enhancing molecular entanglement, and augmenting resistance to jet elongation during electrospinning are linked to the generation of larger-diameter fibers [56]. During the electrospinning experiment, a high flow rate of 5.7 mL/h of the PLA/PEO/KH solution was required. Also, it has been reported that the KH exhibits an average particle size of 1822 nm measured using a Zetasizer Nano-ZS device [23]. The stripe motifs were observed in the case of PVP/CH nanofibers (Figure 2d). Large sizes (1300 ± 840 nm) were obtained for the assembled biomaterial (Figure 2e). This can be explained by the multilayers deposited onto the support and the possibility of trapping CH inside the fibers.

Figure 3 and Table 3 display the energy-dispersive X-ray (EDS) patterns of nanofibers along with their elemental compositions.

Table 3. Compositions of mass and atomic constituents in the electrospun nanofibers.

Element	PLA/PEO		PLA/PEO/KH		PLA/PEO/PVP		PVP/CH		PLA/PEO/KH-PVP/CH	
	Weight (%)	Atomic (%)	Weight (%)	Atomic (%)	Weight (%)	Atomic (%)	Weight (%)	Atomic (%)	Weight (%)	Atomic (%)
Carbon (C)	65.81	76.55	49.54	67.18	58.51	70.83	37.77	55.81	49.46	60.41
Nitrogen (N)	9.63	9.60	0.38	0.44	11.19	11.61	5.94	7.53	0.71	0.74
Oxygen (O)	10.37	9.05	10.33	10.52	11.21	10.19	4.20	4.66	37.17	34.08
Natrium (Na)							1.69	1.31		
Aluminum (Al)	8.17	4.23	35.28	21.30	12.33	6.64	44.34	29.17	7.72	4.20
Chloride (Cl)							1.61	0.81	3.76	0.28
Sulfur (S)			0.04	0.02					0.04	0.02
Iron (Fe)					0.30	0.08	0.50	0.16		
Copper (Cu)	0.92	0.20	1.01	0.26	1.11	0.25	1.03	0.29	1.14	0.26
Gold (Au)	5.10	0.36	3.42	0.28	5.36	0.40	2.92	0.26	3.76	0.28

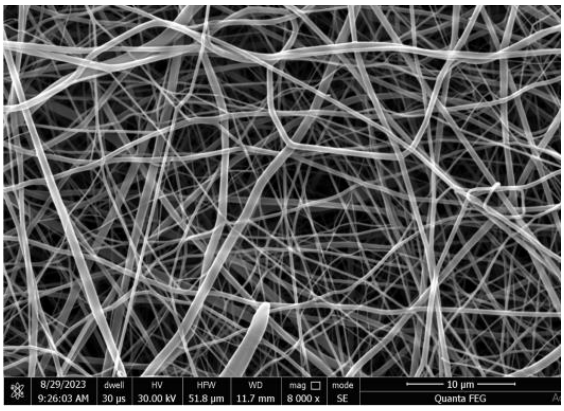

(**a**)

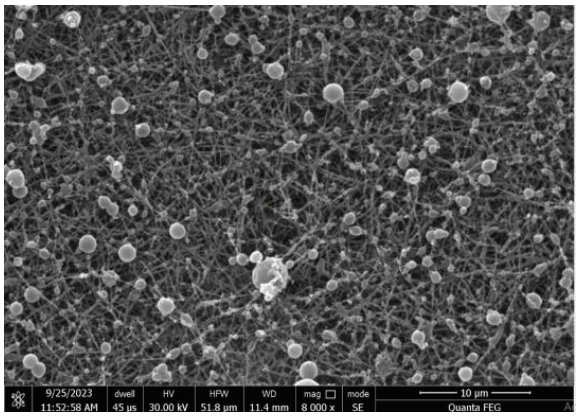

(**b**)

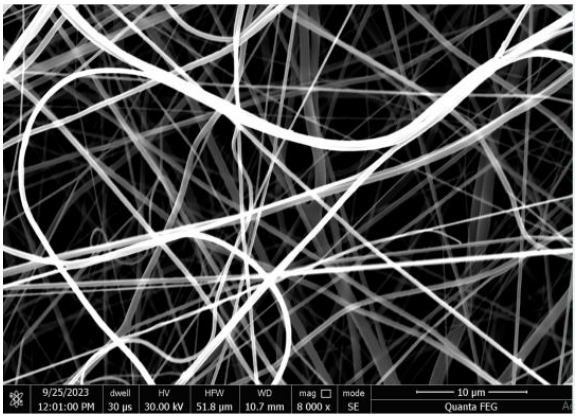

(**c**)

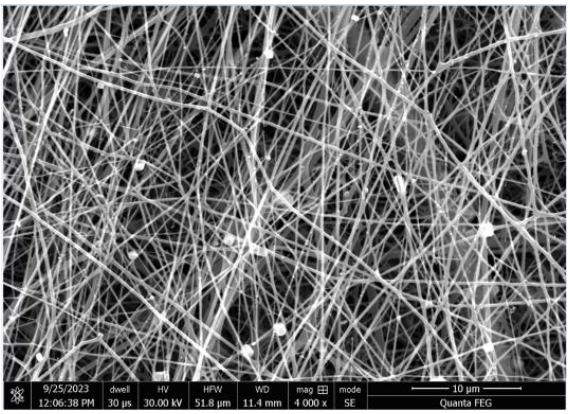

(**d**)

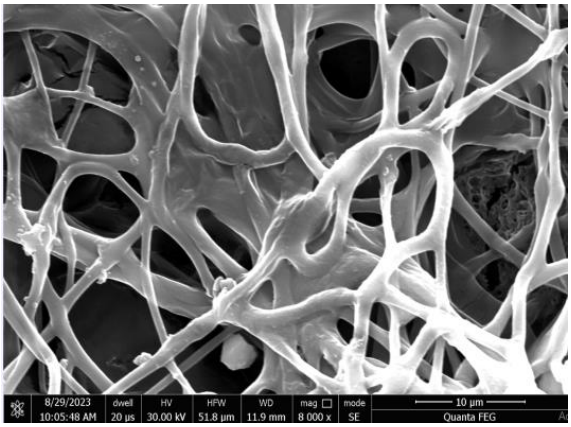

(**e**)

Figure 2. Images captured using Scanning Electron Microscopy (SEM) for: PLA/PEO nanofibers (**a**), PLA/PEO/KH nanofibers (**b**), PLA/PEO/PVP nanofibers (**c**), PVP/CH nanofibers (**d**), and PLA/PEO/KH-PVP/CH nanofibers (**e**).

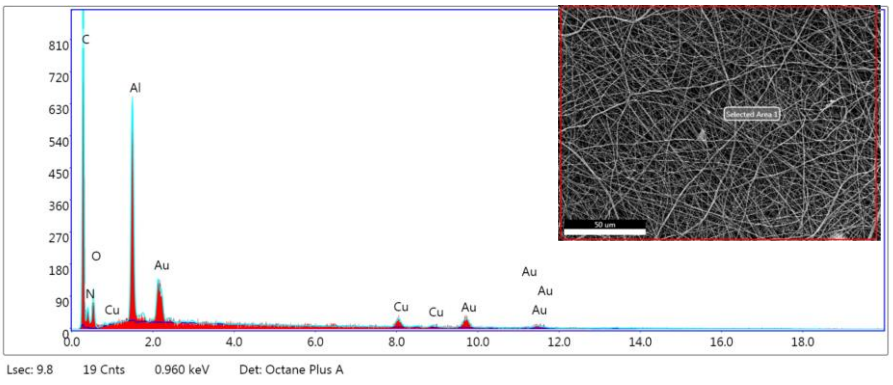

(**a**)

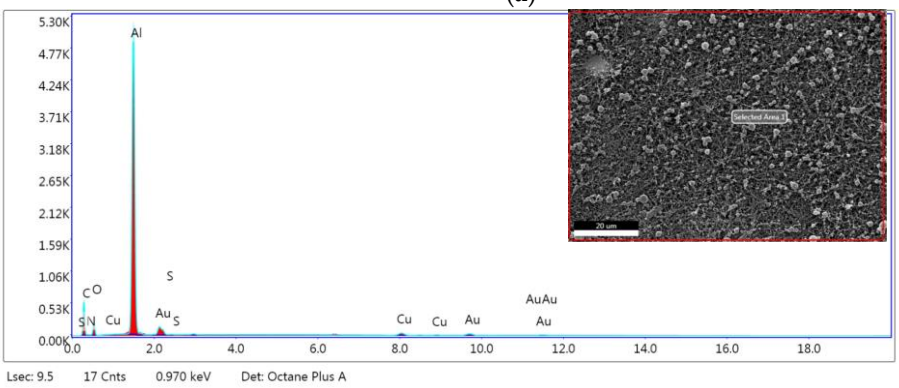

(**b**)

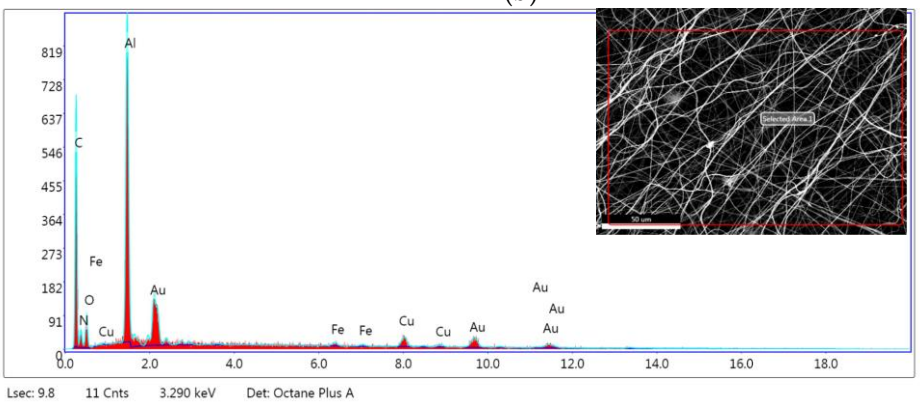

(**c**)

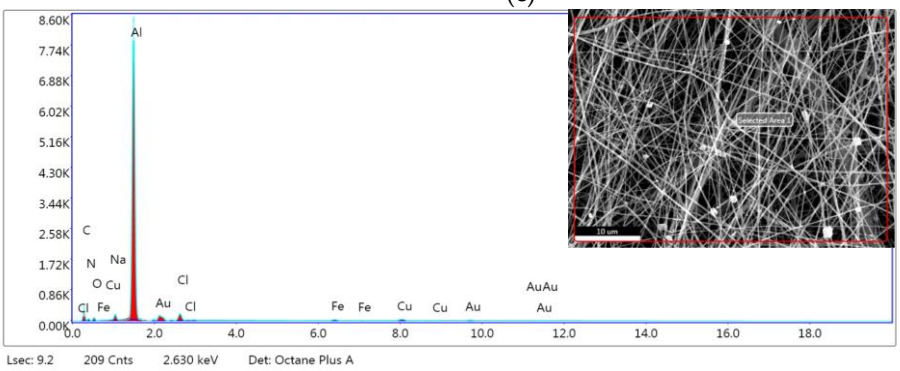

(**d**)

Figure 3. *Cont*.

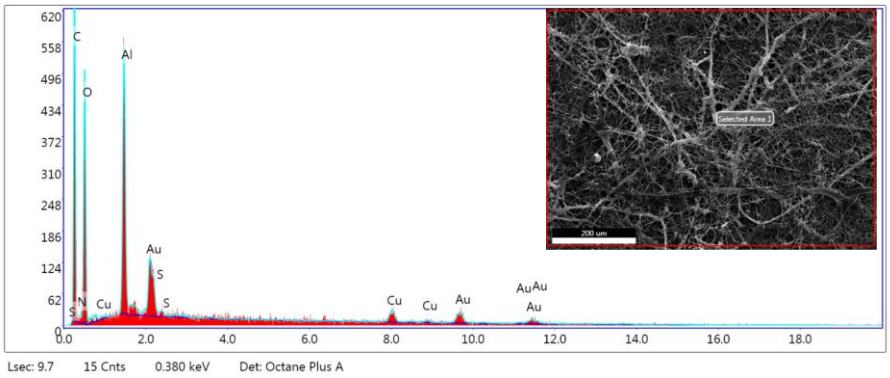

(**e**)

Figure 3. EDS patterns for: PLA/PEO nanofibers: (**a**), PLA/PEO/KH nanofibers (**b**), PLA/PEO/PVP nanofibers (**c**), PVP/CH nanofibers (**d**), and PLA/PEO/KH-PVP/CH nanofibers (**e**).

The EDS elemental data for PLA/PEO nanofibers indicated the presence of carbon (C) and oxygen (O) in high amounts and nitrogen (N), which can be provided from synthesis. The introduction of KH into PLA/PEO revealed the presence of N and sulfur (S). The elemental composition of PLA/PEO/KH-PVP/CH confirms the presence of N and S attributed to the protein structure, and C and O, as the main chemical elements from polymeric matrices.

3.2. ATR-FT-IR Measurements

The FTIR spectra of the samples were analyzed in order to assess the presence of functional groups associated with KH, CH, PLA, PVP, PEO, and PVP and their interaction in the assembled biomaterial (Figure 4).

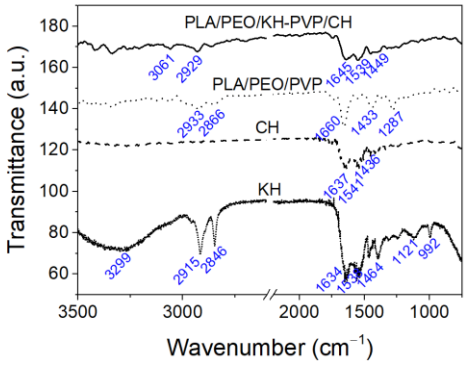

Figure 4. ATR-FT-IR spectra of KH, CH, and PLA/PEO/PVP nanofibers and PLA/PEO/KH-PVP/CH biomaterial.

The ATR-FTIR analysis conducted for keratin hydrolysate shows the presence of a significant band around 3299 cm^{-1}, which corresponds to the stretching vibration exhibited by N-H groups (Amide A band). The stretching vibration of C=O groups (Amide I band) corresponding to the α helix structure [57] was noticed at 1634 cm^{-1} for KH, 1637 cm^{-1} for CH, and 1645 cm^{-1} for the PLA/PEO/KH-PVP/CH biomaterial. The N-H in-plane bending characteristic of β-sheet (Amide II band) conformation [23,57,58] was viewed at 1533 cm^{-1} for KH, 1541 cm^{-1} for CH, and 1539 cm^{-1} for the PLA/PEO/KH-PVP/CH biomaterial. The Amide III band specific to the protein structure was revealed at 1464 cm^{-1} for KH, 1436 cm^{-1} for CH, and 1449 cm^{-1} for the PLA/PEO/KH-PVP/CH biomaterial. The presence of peaks at 2915 cm^{-1} and 2846 cm^{-1} in the KH has been associated with the

antisymmetric and symmetrical stretching vibrations of the C-H bond, respectively. These were shifted to 3061 cm^{-1} and 2866 cm^{-1} for the PLA/PEO/KH-PVP/CH biomaterial. The absorption peaks located at 992 cm^{-1} and 1121 cm^{-1} were associated with the C-SH and $cySO_2$-S-Cy groups found in the KH structure [40]. The band at 1386 cm^{-1} observed in KH is associated with the CH_3 vibration's bending deformation in the amino acid [59]. The FT-IR spectrum of the PLA/PEO/PVP nanofibers revealed absorption bands at 1660 cm^{-1}, 1433 cm^{-1}, and 1287 cm^{-1}, which were attributed to the dipole C=O group within the PVP structure, the CH_3 group with sp^3 hybridization from PLA, and the vibration of the cyanide (CN) stretching within the lactam ring of PLA, respectively [60].

3.3. Antioxidant Activity

The antioxidant activity of PLA/PEO/KH-PVP/CH nanofibers measured through the ABTS radical scavenging bioassay was 97% ± 5.4%. The PLA/PEO/PVP layer was measured for antioxidant activity with no recorded data for this property. HC and KH are responsible for the antioxidant activity, and could have potential benefits for skin health.

Other papers have reported both high antioxidant activity of collagen hydrolysate [61,62] and a lack of antioxidant activity [63]. This behavior could be attributed to the protein extraction conditions, as well as the functional groups of amino acid and peptides available in the protein hydrolysates.

3.4. Controlled Release of Proteins

The cumulative release of KH protein from PLA/PEO/KH-PVP/CH nanofibers indicated the following data for 5 min, 10 min, and 60 min of immersion in distilled water: 4.5% ± 0.3%, 5.8% ± 0.2%, and 7.6% ± 1%, respectively (Figure 5).

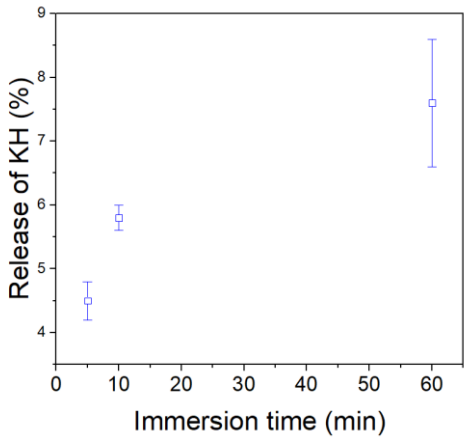

Figure 5. The cumulative release of KH in time, up to 60 min. The dots represents the % of HK released at different times.

The approach to encapsulate CH on the PVP shell layer will ensure a direct contact between the wound and the protein, allowing its beneficial effects on wound healing to take place. The PVP layer can act as a controlled release system for the CH. The use of PVP-based biomaterials as polymeric modifiers in drug delivery systems has been reported [64,65]. Due to its good water solubility [65], the PVP layer readily absorbs wound moisture. It gradually dissolves or releases the encapsulated collagen hydrolysate onto the wound surface. This helps create a moist wound-healing environment, which is known to accelerate wound healing [42]. A moist environment prevents the wound from drying out and promotes cell migration, angiogenesis, and collagen deposition, all of which are essential for proper wound healing [66]. Also, the PLA/PEO matrices will allow for a gradual release of KH from the first layer of the assembled biomaterial. This sustained release of KH and CH ensures that the wound is continuously exposed to proteins' therapeutic effects, aiding in tissue repair and regeneration.

Hajikhani et al. [60] demonstrated accelerated wound closure using a scaffold composed of a core of PLA/PEO loaded with cefazolin and a shell of PVP loaded with collagen due to the controlled release of the antibiotic enabled by the PEO matrix.

3.5. In Vitro Cytocompatibility

The quantitative MTT assay results showed a significant level of cytocompatibility for all tested nanofiber samples (Figure 6). Following 24 h of cell incubation with the samples, cell viability exceeded 80%, indicating a non-cytotoxic effect. Cell viability ranged from 89.29% for PLA/PEO/KH-PVP/CH to 99.77% for PLA/PEO. After 72 h, cell viability slightly increased for almost all the samples, with values surpassing 90%. The highest recorded percentage of cell viability was observed for PLA/PEO/KH (97.87%), while PLA/PEO/KH-PVP/CH exhibited a percentage of 90.88% (as shown in Figure 6).

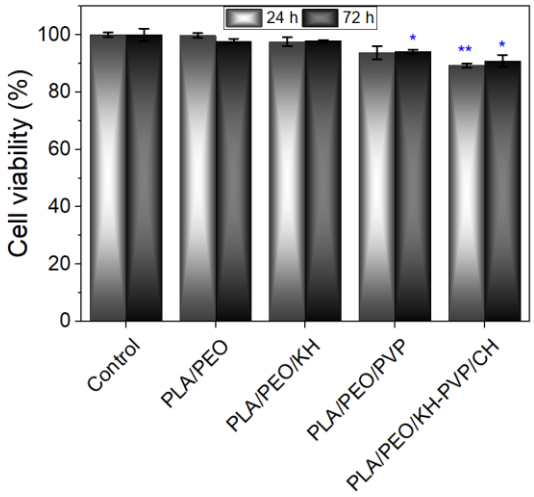

Figure 6. The results of the MTT assay used to assess the viability of NCTC murine fibroblasts grown alongside the nanofibers for 24 h and 72 h. The results are compared to the control, which consisted of cells grown in a fresh culture medium and was considered to have 100% viability. The data are presented as the average value with its corresponding standard deviation (n = 3). The significance for * and ** is that $p < 0.05$ and <0.01, respectively.

This study also examined the morphological characteristics of NCTC cells grown in the presence of nanofiber samples. Following Giemsa staining, the cells were observed under a light microscope. After 72 h of treatment, the cells retained their typical morphology, which closely resembled that of the control. They displayed a fibroblast-like phenotype characterized by a well-defined cytoplasm, cytoplasmic extensions, and euchromatic nuclei with multiple nucleoli (Figure 7). The cell density in the treated nanofiber samples was comparable to that of the control, with cells covering approximately 85% to 90% of the well's surface.

Overall, the morphological findings were in good agreement with the outcomes of the quantitative MTT test, indicating that there was no cytotoxic effect of all tested nanofiber samples on NCTC cells.

Other papers related to the valorization of collagen extracted from animal by-products for medical applications have reported a good biocompatibility [23,24,67,68]. Similarly, Ramirez et al. [69] successfully developed two fibrous layers using polyvinyl alcohol (PVA) and wool-keratin for wound healing purposes, demonstrating a noteworthy enhancement of the in vitro cell adhesion.

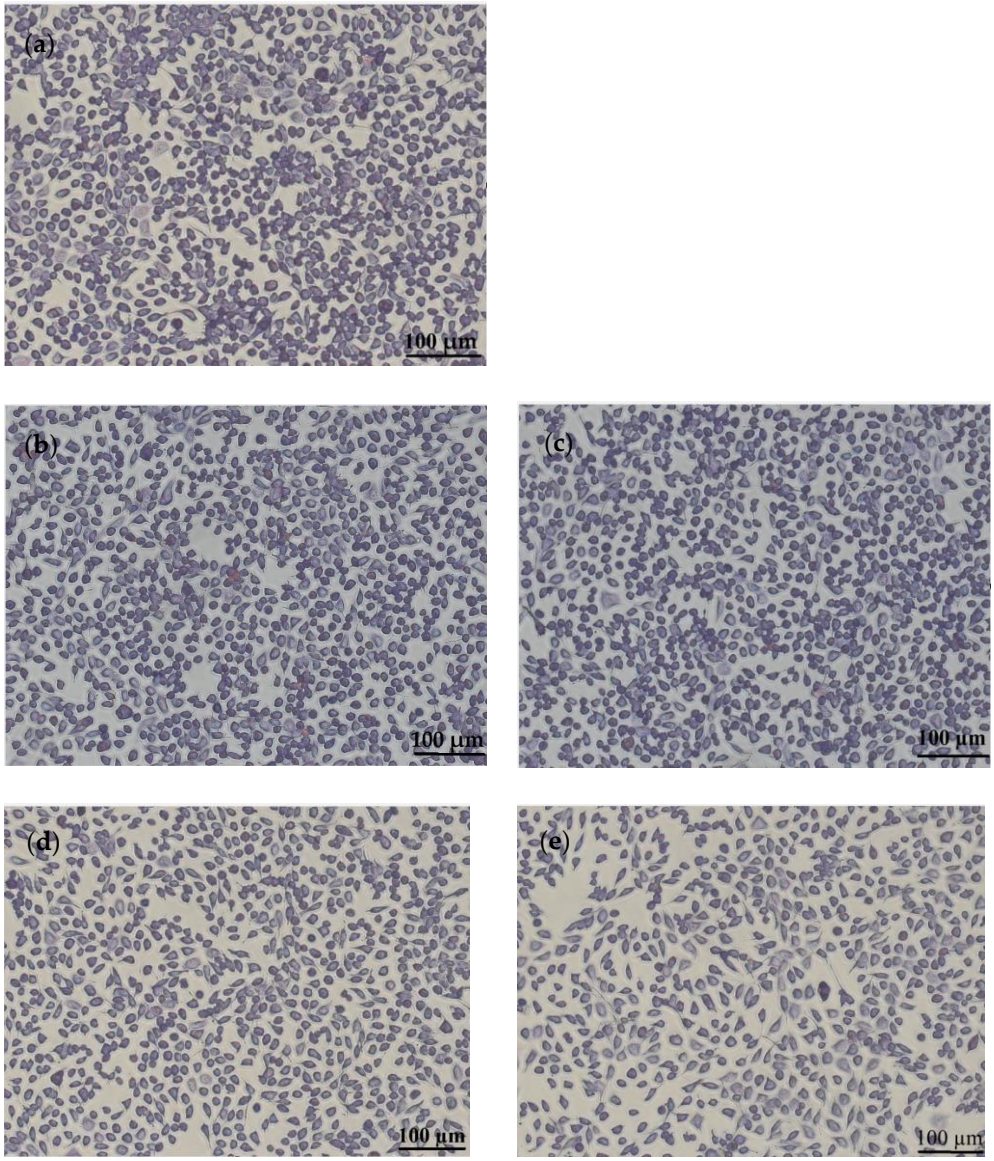

Figure 7. Light micrographs of NCTC mouse fibroblasts treated for 72 h with: (**a**) Culture medium; (**b**) PLA/PEO nanofibers; (**c**) PLA/PEO/KH nanofibers; (**d**) PLA/PEO/PVP nanofibers; and (**e**) PLA/PEO/KH-PVP/CH nanofibers. Scale bare = 100 µm (Giemsa staining).

3.6. In Vivo Biocompatibility Tests

During the monitoring period, no behavioral changes were detected in the behavior of the animals that received the investigated nanofibers. The mice exhibited typical behaviors such as exploring their environment, eating, drinking, and personal hygiene. On the seventh day of the study, the patches were taken off, and the incision area was examined macroscopically. It was observed that, in both the animals of the control group and those exposed to PLA/PEO, PLA/PEO/KH, PLA/PEO/PVP, PVP/CH, and PLA/PEO/KH-PVP/CH electrospun nanofibers, the integuments had a normal appearance and no signs of inflammation, and the incision area was completely cicatrized.

3.6.1. Leukocyte Formula Elements

Table 4 shows the proportion of the various components (neutrophil polymorphonuclear (PMN), lymphocytes (Ly), eosinophils (E), monocytes (M), and basophils (B)) within the leukocyte formula of the animals subjected to electrospun nanofibers compared to the control group (designated as a witness), both at the 24 h and 7-day marks.

Table 4. Percentage values of leukocyte formula elements measured in animals that received nanofibers. The findings are displayed as the average value with its corresponding standard deviation, representing percentages for each element, based on data obtained from five mice per batch.

	Duration	**Leukocyte Differential Count (%)**				
		PMN	**Ly**	**E**	**M**	**B**
Witness	24 h	29.4 ± 7.7	63.9 ± 18.3	0.1 ± 0.01	6.1 ± 1.1	0.2 ± 0.05
	7 d	28.6 ± 8.9	64.8 ± 19.5	0.2 ± 0.05	6.2 ± 1.1	0.2 ± 0.05
PLA/PEO	24 h	28.5 ± 8.5	65.0 ± 17.5	0.2 ± 0.05	6.1 ± 1.3	0.2 ± 0.05
	7 d	28.7 ± 9.1	64.6 ± 18.7	0.2 ± 0.01	6.3 ± 1.3	0.2 ± 0.1
PLA/PEO/KH	24 h	29.2 ± 8.3	64.1 ± 18.9	0.1 ± 0.01	6.4 ± 0.5	0.2 ± 0.1
	7 d	28.9 ± 9.3	64.5 ± 18.3	0.1 ± 0.01	6.3 ± 1.1	0.2 ± 0.05
PLA/PEO/PVP	24 h	29.3 ± 7.9	64.3 ± 17.9	0.1 ± 0.05	6.1 ± 1.1	0.2 ± 0.1
	7 d	29.1 ± 8.7	64.4 ± 19.1	0.1 ± 0.01	6.2 ± 1.3	0.2 ± 0.1
PVP/CH	24 h	28.6 ± 8.5	64.8 ± 18.5	0.2 ± 0.01	6.2 ± 1.1	0.2 ± 0.1
	7 d	27.8 ± 8.9	64.5 ± 18.7	0.1 ± 0.05	6.3 ± 1.3	0.2 ± 0.05
PLA/PEO/KH-PVP/CH	24 h	28.6 ± 8.7	65.6 ± 18.9	0.1 ± 0.01	6.3 ± 1.1	0.2 ± 0.05
	7 d	28.8 ± 9.1	64.4 ± 17.7	0.2 ± 0.05	6.4 ± 0.5	0.2 ± 0.1

Hematological investigations revealed that there were no noteworthy differences in the percentage values of the leukocyte differential count (PMN, Ly, E, M, and B) in animals treated with nanofibers when compared to the control group after 24 h and 7 days of the study. These results suggest that covering the incision area with simple patches, or patches containing nanofibers, prevented the development of both local and systemic inflammatory reactions.

3.6.2. Liver Enzymes

Table 5 shows the serum levels of glutamic-oxaloacetic transaminase (TGO), glutamic-pyruvic transaminase (TGP), and lactate dehydrogenase (LDH) for mice that received electrospun nanofiber samples.

Table 5. Changes in serum levels of TGP, TGO, and LDH in animals subjected to nanofibers administration. The findings are displayed as the average value with its corresponding standard deviation representing the TGP, TGO, and LDH values for five mice per batch.

	Duration	**TGP (U/mL)**	**TGO (U/mL)**	**LDH (U/L)**
Witness	24 h	39.6 ± 10.3	158.6 ± 31.5	328.28 ± 64.33
	7 d	40.2 ± 10.5	160.4 ± 30.7	333.56 ± 70.67
PLA/PEO	24 h	40.5 ± 10.9	161.7 ± 32.9	332.34 ± 71.13
	7 d	40.7 ± 10.7	163.2 ± 33.7	335.83 ± 66.83
PLA/PEO/KH	24 h	39.4 ± 9.7	159.8 ± 35.3	330.45 ± 69.45
	7 d	40.3 ± 10.5	161.3 ± 32.7	334.32 ± 58.83
PLA/PEO/PVP	24 h	40.6 ± 11.3	158.5 ± 33.5	331.27 ± 72.13
	7 d	39.8 ± 9.9	162.7 ± 31.7	335.19 ± 71.33
PVP/CH	24 h	39.5 ± 10.7	160.6 ± 34.1	332.53 ± 67.67
	7 d	39.8 ± 10.3	163.8 ± 33.5	336.13 ± 69.27
PLA/PEO/KH-PVP/CH	24 h	39.7 ± 10.5	160.4 ± 35.3	330.67 ± 71.33
	7 d	40.5 ± 11.1	161.3 ± 30.9	333.21 ± 70.67

The results from Table 5 show that no substantial differences in TGP, TGO, or LDH activity, the common liver enzymes, were detected between mice treated with PLA/PEO, PLA/PEO/KH, PLA/PEO/PVP, PVP/CH, and PLA/PEO/KH-PVP/CH and those of

the witness after 24 h and 7 days of the study. Table 6 shows insignificant differences for urea and creatinine in the case of samples as compared to control sample. These results constitute arguments on the fact that the use of nanofibers did not produce disturbances in the liver function of laboratory animals.

Table 6. Modifications in the blood urea and creatinine levels observed in animals receiving nanofibers. The findings are displayed as the average value with its corresponding standard deviation representing the urea and creatinine values for five mice per batch.

	Duration	Urea (mg/dL)	Creatinine (mg/dL)
Witness	24 h	27.7 ± 3.7	0.7 ± 0.01
	7 d	28.3 ± 4.3	0.7 ± 0.03
PLA/PEO	24 h	26.9 ± 4.7	0.8 ± 0.03
	7 d	28.5 ± 4.5	0.9 ± 0.05
PLA/PEO/KH	24 h	29.1 ± 5.3	0.8 ± 0.01
	7 d	29.5 ± 4.9	0.8 ± 0.01
PLA/PEO/PVP	24 h	29.1 ± 5.1	0.7 ± 0.01
	7 d	28.9 ± 3.7	0.9 ± 0.03
PVP/CH	24 h	29.3 ± 4.5	0.8 ± 0.03
	7 d	29.7 ± 4.9	0.8 ± 0.05
PLA/PEO/KH-PVP/CH	24 h	29.5 ± 4.7	0.9 ± 0.01
	7 d	28.7 ± 5.3	0.8 ± 0.03

The application of patches containing nanofibers over the incision area did not result in noticeable changes in the serum levels of urea and creatinine when compared to the use of simple patches at the specified time determinations. These findings suggest that the use of nanofibers did not cause any disturbances in renal function.

Table 7 shows the blood levels of superoxide dismutase (SOD) and glutathione peroxidase (GPx) in mice that received electrospun nanofiber samples.

Table 7. Modifications in the activity of SOD and GPx observed in animals subjected to nanofibers administration. The findings are displayed as the average value with its corresponding standard deviation representing the SOD and GPx values for five mice per batch.

	Duration	SOD (U/mg Protein)	GPX (μm/mg Protein)
Witness	24 h	103.6 ± 16.5	13.1 ± 2.3
	7 d	105.2 ± 19.7	12.3 ± 1.7
PLA/PEO	24 h	103.5 ± 18.3	12.7 ± 1.3
	7 d	104.6 ± 18.5	13.3 ± 1.9
PLA/PEO/KH	24 h	104.7 ± 17.7	13.5 ± 2.1
	7 d	104.4 ± 19.3	12.7 ± 1.5
PLA/PEO/PVP	24 h	104.2 ± 19.1	12.9 ± 1.7
	7 d	105.8 ± 20.3	12.3 ± 1.1
PVP/CH	24 h	103.1 ± 18.7	13.1 ± 2.5
	7 d	105.5 ± 17.9	13.3 ± 1.7
PLA/PEO/KH-PVP/CH	24 h	104.8 ± 19.1	12.7 ± 1.5
	7 d	105.4 ± 19.5	13.5 ± 1.3

There were no notable variations in the serum SOD and GPx values of the tested nanofiber-treated mice when compared to the control group, both after 24 h and 7 days of

testing. Therefore, the application of nanofibers did not significantly influence the oxidative processes in the duration of the study.

3.6.3. Immunological Tests

The study examined the impact of PLA/PEO, PLA/PEO/KH, PLA/PEO/PVP, PVP/CH, and PLA/PEO/KH-PVP/CH nanofibers on incision areas in animals. After a 7-day period, there were no significant variations observed in serum opsonic capacity (OC), phagocytic capacity (PC), and bactericidal capacity (BC) levels when compared to a control group of animals (Table 8). These pieces of evidence reveal that the use of nanofibers did not induce changes in the immune defense capacity of the tested animals.

Table 8. Modification in the OC, PC, and BC values in animals subjected to nanofibers administration. The findings are displayed as the average value with its corresponding standard deviation representing the OC, PC, and BC values for five mice per batch.

	Duration	OC (Colonies/mL)	PC (Colonies/mL)	BC (Colonies/mL)
Witness	7 d	769.83 ± 65.27	529.37 ± 41.17	713.56 ± 62.21
PLA/PEO	7 d	773.13 ± 61.43	531.41 ± 39.33	718.34 ± 65.37
PLA/PEO/KH	7 d	785.45 ± 67.45	525.29 ± 38.25	717.55 ± 60.33
PLA/PEO/PVP	7 d	794.33 ± 70.21	522.13 ± 40.21	714.21 ± 53.67
PLA/PEO/KH-PVP/CH	7 d	788.29 ± 62.83	530.67 ± 33.83	721.82 ± 57.17

All studies conducted in controlled laboratory settings demonstrated that the use of nanofibers containing bovine collagen and keratin hydrolysates, which were incorporated into eco-friendly polymers, did not produce noteworthy modifications in hematological, biochemical, or immunological tests. Also, the developed nanofibers did not significantly influence some specific oxidative stress parameters when compared to patches with a textile support. These findings suggest a good in vivo biocompatibility and indicate the potential utility of the tested systems.

4. Conclusions

In this paper, a dual-layer biomaterial with a nanofibrous structure was fabricated using both mono and coaxial electrospinning techniques. The results showed a nanofibrous structure in each layer, along with a positive effect of antioxidant activity, controlled release of protein-derived animals, and a high degree of in vitro and vivo biocompatibility of the assembled product, suggesting its potential suitability for wound dressings applications.

The research will continue with additional in vitro and in vivo investigations including scratch assays, migration assays, evaluation of cytokine and growth factor release, wound closure assessments, histological analyses, and functional recovery. Also, the second layer can be designed to possess antimicrobial properties, reducing the risk of wound infections. By further assessing the properties of the PLA/PEO/KH-PVP/CH biomaterial created for covering wounds resulting from skin burns, significant advantages are expected to be achieved, such as infection prevention, moisture retention, enhanced barrier function, easy adhesion of dressing, and improved patient comfort during the healing process.

Author Contributions: Conceptualization, C.G. and M.R.; Formal analysis, E.M. and A.C.B.; Funding acquisition, C.P.; Investigation, C.G., M.R., L.M.S., A.C.B. and L.M.-T.; Methodology, M.R., E.M. and C.P.; Resources, L.M.S. and C.P.; Software, A.C.B.; Supervision, A.C.B.; Validation, C.G., A.C.B. and L.M.-T.; Visualization, C.G. and E.M.; Writing—original draft, C.G., M.R., L.M.S., E.M. and L.M.-T.; Writing—review and editing, M.R. and L.M.S. All authors have read and agreed to the published version of the manuscript.

Funding: This research was funded by a grant from the Romanian Ministry of Research, Innovation and Digitalization, CCCDI-UEFISCDI, project no. PN-III-P3-3.5-EUK-2019-0237 within PNCDI III (NonActiv-Pans), Contract 219/23.12.2020.

Data Availability Statement: The data presented in this study are available on request from the corresponding author.

Acknowledgments: In Vitro Cytocompatibility tests were performed under the Programme Nucleu, within the National Research, Development and Innovation Plan 2022–2027, carried out with the support of Romanian Ministry of Research, Innovation and Digitalization, Contract 7N/03.01.2023, Project no. 23020101. The FTIR analysis (on INTERSPEC 200-X Spectrophotometer) was possible due to European Regional Development Fund through Competitiveness Operational Program 2014–2020, Priority axis 1, Project No. P_36_611, MySMIS code 107066, Innovative Technologies for Materials Quality Assurance in Health, Energy and Environmental—Center for Innovative Manufacturing Solutions of Smart Biomaterials and Biomedical Surfaces-INOVABIOMED.

Conflicts of Interest: The authors declare no conflict of interest.

References

1. Crops and Livestock Products. Available online: http://www.fao.org/faostat/en/#data/QA (accessed on 13 August 2023).
2. Mokrejs, P.; Langmaier, F.; Mladek, M.; Janacova, D.; Kolomaznik, K.; Vasek, V. Extraction of collagen and gelatine from meat industry by-products for food and non food uses. *Waste Manag. Res.* **2009**, *27*, 31–37. [CrossRef]
3. Singaravelu, S.; Ramanathan, G.; Sivagnanam, U.T. Dual-layered 3D nanofibrous matrix incorporated with dual drugs and their synergetic effect on accelerating wound healing through growth factor regulation. *Mater. Sci. Eng. C-Mater. Biol. Appl.* **2017**, *76*, 37–49. [CrossRef] [PubMed]
4. Corchero, J.L.; Favaro, M.T.P.; Marquez-Martinez, M.; Lascorz, J.; Martinez-Torro, C.; Sanchez, J.M.; Lopez-Laguna, H.; de Souza Ferreira, L.C.; Vazquez, E.; Ferrer-Miralles, N.; et al. Recombinant Proteins for Assembling as Nano- and Micro-Scale Materials for Drug Delivery: A Host Comparative Overview. *Pharmaceutics* **2023**, *15*, 1197. [CrossRef]
5. Arun, A.; Malrautu, P.; Laha, A.; Luo, H.; Ramakrishna, S. Collagen Nanoparticles in Drug Delivery Systems and Tissue Engineering. *Appl. Sci.* **2021**, *11*, 1369. [CrossRef]
6. Willoughby, C.E.; Batterbury, M.; Kaye, S.B. Collagen corneal shields. *Surv. Ophthalmol.* **2002**, *47*, 174–182. [CrossRef] [PubMed]
7. Shokrani, H.; Shokrani, A.; Sajadi, S.M.; Seidi, F.; Mashhadzadeh, A.H.; Rabiee, N.; Saeb, M.R.; Aminabhavi, T.; Webster, T.J. Cell-Seeded Biomaterial Scaffolds: The Urgent Need for Unanswered Accelerated Angiogenesis. *Int. J. Nanomed.* **2022**, *17*, 1035–1068. [CrossRef]
8. Samoraj, M.; Mironiuk, M.; Izydorczyk, G.; Witek-Krowiak, A.; Szopa, D.; Moustakas, K.; Chojnacka, K. The challenges and perspectives for anaerobic digestion of animal waste and fertilizer application of the digestate. *Chemosphere* **2022**, *295*, 133799. [CrossRef]
9. Perez-Aguilar, H.; Lacruz-Asaro, M.; Aran-Ais, F. Towards a circular bioeconomy: High added value protein recovery and recycling from animal processing by-products. *Sustain. Chem. Pharm.* **2022**, *28*, 100667. [CrossRef]
10. Broda, J.; Gawlowski, A.; Rom, M.; Kobiela-Mendrek, K. Utilisation of waste wool from mountain sheep as fertiliser in winter wheat cultivation. *J. Nat. Fibers* **2023**, *20*, 1–14. [CrossRef]
11. Alao, B.O.; Falowo, A.B.; Chulayo, A.; Muchenje, V. The Potential of Animal By-Products in Food Systems: Production, Prospects and Challenges. *Sustainability* **2017**, *9*, 1089. [CrossRef]
12. Etemadian, Y.; Ghaemi, V.; Shaviklo, A.R.; Pourashouri, P.; Mahoonak, A.R.S.; Rafipour, F. Development of animal/plant-based protein hydrolysate and its application in food, feed and nutraceutical industries: State of the art. *J. Clean. Prod.* **2021**, *278*, 123219. [CrossRef]
13. Shahzad, K.; Kettl, K.-H.; Titz, M.; Koller, M.; Schnitzer, H.; Narodoslawsky, M. Comparison of ecological footprint for biobased PHA production from animal residues utilizing different energy resources. *Clean Technol. Environ. Policy* **2013**, *15*, 525–536. [CrossRef]
14. Khodaei, D.; Alvarez, C.; Mullen, A.M. Biodegradable Packaging Materials from Animal Processing Co-Products and Wastes: An Overview. *Polymers* **2021**, *13*, 2561. [CrossRef] [PubMed]
15. Saad, V.; Gutschmann, B.; Grimm, T.; Widmer, T.; Neubauer, P.; Riedel, S.L. Low-quality animal by-product streams for the production of PHA-biopolymers: Fats, fat/protein-emulsions and materials with high ash content as low-cost feedstocks. *Biotechnol. Lett.* **2021**, *43*, 579–587. [CrossRef] [PubMed]
16. Masilamani, D.; Madhan, B.; Shanmugam, G.; Palanivel, S.; Narayan, B. Extraction of collagen from raw trimming wastes of tannery: A waste to wealth approach. *J. Clean. Prod.* **2016**, *113*, 338–344. [CrossRef]
17. Tarafdar, A.; Gaur, V.K.; Rawat, N.; Wankhade, P.R.; Gaur, G.K.; Awasthi, M.K.; Sagar, N.A.; Sirohi, R. Advances in biomaterial production from animal derived waste. *Bioengineered* **2021**, *12*, 8247–8258. [CrossRef]
18. Budiatin, A.S.; Gani, M.A.; Nilamsari, W.P.; Ardianto, C.; Khotib, J. The Characterization of Bovine Bone-Derived Hydroxyapatite Isolated Using Novel Non-Hazardous Method. *J. Biomim. Biomater. Biomed. Eng.* **2020**, *45*, 49–56. [CrossRef]
19. Parajuli, K.; Malla, K.P.; Panchen, N.; Ganga, G.C.; Adhikari, R. Isolation of antibacterial nano-hydroxyapatite biomaterial from waste buffalo bone and its characterization. *Chem. Chem. Technol.* **2022**, *16*, 133–141. [CrossRef]

20. Ramesh, S.; Loo, Z.Z.; Tan, C.Y.; Chew, W.J.K.; Ching, Y.C.; Tarlochan, F.; Chandran, H.; Krishnasamy, S.; Bang, L.T.; Sarhan, A.A.D. Characterization of biogenic hydroxyapatite derived from animal bones for biomedical applications. *Ceram. Int.* **2018**, *44*, 10525–10530. [CrossRef]
21. Dragusin, D.M.; Curti, F.; Cecoltan, S.; Sarghiuta, D.; Butac, L.M.; Vasile, E.; Marinescu, R.; Stancu, I.C. Biocomposites Based on Biogenous Mineral for Inducing Biomimetic Mineralization. *Mater. Plast.* **2017**, *54*, 207–213. [CrossRef]
22. Horbert, V.; Xin, L.; Foehr, P.; Brinkmann, O.; Bungartz, M.; Burgkart, R.H.; Graeve, T.; Kinne, R.W. In Vitro Analysis of Cartilage Regeneration Using a Collagen Type I Hydrogel (CaReS) in the Bovine Cartilage Punch Model. *Cartilage* **2019**, *10*, 346–363. [CrossRef] [PubMed]
23. Râpă, M.; Gaidău, C.; Stefan, L.M.; Matei, E.; Niculescu, M.; Berechet, M.D.; Stanca, M.; Tablet, C.; Tudorache, M.; Gavrilă, R.; et al. New nanofibers based on protein by-products with bioactive potential for tissue engineering. *Materials* **2020**, *13*, 3149. [CrossRef]
24. Matei, E.; Gaidau, C.; Rapa, M.; Constantinescu, R.; Savin, S.; Berechet, M.D.; Predescu, A.M.; Berbecaru, A.C.; Coman, G.; Predescu, C. Sustainable Rabbit Skin Glue to Produce Bioactive Nanofibers for Nonactive Wound Dressings. *Materials* **2020**, *13*, 5388. [CrossRef]
25. Giteru, S.G.G.; Ramsey, D.H.H.; Hou, Y.; Cong, L.; Mohan, A.; El-Din Ahmed Bekhit, A. Wool keratin as a novel alternative protein: A comprehensive review of extraction, purification, nutrition, safety, and food applications. *Compr. Rev. Food Sci. Food Saf.* **2023**, *22*, 643–687. [CrossRef]
26. Athwal, S.; Sharma, S.; Gupta, S.; Nadda, A.K.; Gupta, A.; Husain, M.S.B. Sustainable Biodegradation and Extraction of Keratin with Its Applications. In *Handbook of Biopolymers*; Thomas, S., AR, A., Jose Chirayil, C., Thomas, B., Eds.; Springer Nature Singapore Pte Ltd.: Singapore, 2022; p. 25302740.
27. Perta-Crisan, S.; Ursachi, C.S.; Gavrilas, S.; Oancea, F.; Munteanu, F.-D. Closing the Loop with Keratin-Rich Fibrous Materials. *Polymers* **2021**, *13*, 1896. [CrossRef]
28. Majeed, Z.; Farhat, H.; Ahmad, B.; Iqbal, A.; Faiz, A.U.H.; Mahnashi, M.H.; Alqarni, A.O.; Alqahtani, O.; Ali, A.A.; Momenah, A.M. Process optimization, antioxidant, antibacterial, and drug adjuvant properties of bioactive keratin microparticles derived from porcupine (Hystrix indica) quills. *PeerJ* **2023**, *11*, e15653. [CrossRef] [PubMed]
29. Santhanam, R.; Rameli, M.A.P.; Al Jeffri, A.; Ismail, W.I.W. Bovine Based Collagen Dressings in Wound Care Management. *J. Pharm. Res. Int.* **2020**, *32*, 48–63. [CrossRef]
30. Wang, Q.; Ma, J.; Chen, S.; Wu, S. Designing an Innovative Electrospinning Strategy to Generate PHBV Nanofiber Scaffolds with a Radially Oriented Fibrous Pattern. *Nanomaterials* **2023**, *13*, 1150. [CrossRef]
31. Wang, P.; Lv, H.; Cao, X.; Liu, Y.; Yu, D.-G. Recent Progress of the Preparation and Application of Electrospun Porous Nanofibers. *Polymers* **2023**, *15*, 921. [CrossRef]
32. Gomaa, S.F.; Madkour, T.M.; Moghannem, S.; El-Sherbiny, I.M. New polylactic acid/ cellulose acetate-based antimicrobial interactive single dose nanofibrous wound dressing mats. *Int. J. Biol. Macromol.* **2017**, *105*, 1148–1160. [CrossRef]
33. Yang, Q.B.; Li, Z.Y.; Hong, Y.L.; Zhao, Y.Y.; Qiu, S.L.; Wang, C.; Wei, Y. Influence of solvents on the formation of ultrathin uniform poly(vinyl pyrrolidone) nanofibers with electrospinning. *J. Polym. Sci. Part B-Polym. Phys.* **2004**, *42*, 3721–3726. [CrossRef]
34. Mahapatro, A.; Singh, D.K. Biodegradable nanoparticles are excellent vehicle for site directed in-vivo delivery of drugs and vaccines. *J. Nanobiotechnol.* **2011**, *9*, 55. [CrossRef]
35. Gaudreault, R.; Whitehead, M.A.; van de Ven, T.G.M. Molecular orbital studies of gas-phase interactions between complex molecules. *J. Phys. Chem. A* **2006**, *110*, 3692–3702. [CrossRef] [PubMed]
36. Sreekanth, K.; Siddaiah, T.; Gopal, N.O.; Kumar, Y.M.; Ramu, C. Optical and electrical conductivity studies of VO2+ doped polyvinyl pyrrolidone (PVP) polymer electrolytes. *J. Sci.-Adv. Mater. Devices* **2019**, *4*, 230–236. [CrossRef]
37. Mbese, Z.; Alven, S.; Aderibigbe, B.A. Collagen-Based Nanofibers for Skin Regeneration and Wound Dressing Applications. *Polymers* **2021**, *13*, 4368. [CrossRef]
38. Goh, P.S.; Othman, M.H.D.; Matsuura, T. Waste Reutilization in Polymeric Membrane Fabrication: A New Direction in Membranes for Separation. *Membranes* **2021**, *11*, 782. [CrossRef]
39. Gaidau, C.; Niculescu, M.; Stepan, E.; Taloi, D.; Filipescu, L. Additives and Advanced Biomaterials Obtained from Leather Industry by-products. *Rev. Chim.* **2009**, *60*, 501–507.
40. Gaidau, C.; Stanca, M.; Niculescu, M.D.; Alexe, C.A.; Becheritu, M.; Horoias, R.; Cioineag, C.; Rapa, M.; Stanculescu, I.R. Wool Keratin Hydrolysates for Bioactive Additives Preparation. *Materials* **2021**, *14*, 4696. [CrossRef]
41. Keirouz, A.; Wang, Z.; Reddy, V.S.; Nagy, Z.K.; Vass, P.; Buzgo, M.; Ramakrishna, S.; Radacsi, N. The History of Electrospinning: Past, Present, and Future Developments. *Adv. Mater. Technol.* **2023**, *8*, 2201723. [CrossRef]
42. Darie-Nita, R.N.; Rapa, M.; Frackowiak, S. Special Features of Polyester-Based Materials for Medical Applications. *Polymers* **2022**, *14*, 951. [CrossRef]
43. Croitoru, A.M.; Karacelebi, Y.; Saatcioglu, E.; Altan, E.; Ulag, S.; Aydogan, H.K.; Sahin, A.; Motelica, L.; Oprea, O.; Tihauan, B.M.; et al. Electrically Triggered Drug Delivery from Novel Electrospun Poly(Lactic Acid)/Graphene Oxide/Quercetin Fibrous Scaffolds for Wound Dressing Applications. *Pharmaceutics* **2021**, *13*, 957. [CrossRef]
44. Rashedi, S.M.; Khajavi, R.; Rashidi, A.; Rahimi, M.K.; Bahador, A. Nanocomposite-Coated Sterile Cotton Gas Based on Polylactic Acid and Nanoparticles (Zinc Oxide and Copper Oxide) and Tranexamic Acid Drug with the Aim of Wound Dressing. *Regen. Eng. Transl. Med.* **2021**, *7*, 200–217. [CrossRef]

45. Fernandes, D.M.; Barbosa, W.S.; Rangel, W.S.P.; Moura, I.; Matos, A.P.D.; Melgaco, F.G.; Dias, M.L.; Ricci, E.; da Silva, L.C.P.; de Abreu, L.C.L.; et al. Polymeric membrane based on polyactic acid and babassu oil for wound healing. *Mater. Today Commun.* **2021**, *26*, 102173. [CrossRef]
46. Li, W.; Wang, J.; Cheng, Z.; Yang, G.; Zhao, C.; Gao, F.; Zhang, Z.; Qian, Y. Sandwich structure Aloin-PVP/Aloin-PVP-PLA/PLA as a wound dressing to accelerate wound healing. *Rsc Adv.* **2022**, *12*, 27300–27308. [CrossRef] [PubMed]
47. Lindstrom, N.M.; Moore, D.M.; Zimmerman, K.; Smith, S.A. Hematologic Assessment in Pet Rats, Mice, Hamsters, and Gerbils Blood Sample Collection and Blood Cell Identification. *Clin. Lab. Med.* **2015**, *35*, 629–640. [CrossRef]
48. Wolf, M.F.; Anderson, J.M. Practical approach to blood compatibility assessments: General considerations and standards. *Biocompat. Perform. Med. Devices* **2012**, *50*, 159–200.
49. Zou, W.S.; Yang, Y.Q.; Gu, Y.; Zhu, P.F.; Zhang, M.J.; Cheng, Z.; Liu, X.Y.; Yu, Y.J.; Peng, X.H. Repeated Blood Collection from Tail Vein of Non-Anesthetized Rats with a Vacuum Blood Collection System. *Jove-J. Vis. Exp.* **2017**, *10*, 5852. [CrossRef]
50. Parasuraman, S.; Raveendran, R.; Kesavan, R. Blood Sample Collection in Small Laboratory Animals (vol 1, pg 87, 2010). *J. Pharmacol. Pharmacother.* **2017**, *8*, 153. [CrossRef]
51. Tranquilli, W.J.; Thurmon, J.C.; Grimm, K.A.; Lumb, W.V. *Lumb & Jones' Veterinary Anesthesia and Analgesia*; Ames, T.E., Ed.; Blackwell Pub.: Ames, IA, USA, 2007; Available online: https://books-library.net/files/books-library.online_noob5781bfd0cd351b04a09bb-58889 (accessed on 26 August 2023).
52. Toft, M.F.; Petersen, M.H.; Dragsted, N.; Hansen, A.K. The impact of different blood sampling methods on laboratory rats under different types of anaesthesia. *Lab. Anim.* **2006**, *40*, 261–274. [CrossRef]
53. Tartau, L.; Cazacu, A.; Melnig, V. Ketoprofen-liposomes formulation for clinical therapy. *J. Mater. Sci.-Mater. Med.* **2012**, *23*, 2499–2507. [CrossRef]
54. Directive 2010/63 / EU of the European Parliament and of the Council of 22 September 2010 on the Protection of Used Animals for Scientific Purposes. Available online: http://eur-lex.europa.eu/legal-content/EN/TXT/?uri=CELEX:32010L0063 (accessed on 20 September 2021).
55. AVMA Guidelines on Euthanasia (Formerly the Report of the AVMA Panel on Euthanasia). 2007. Available online: https://olaw.nih.gov/sites/default/files/Euthanasia2007.pdf (accessed on 20 September 2023).
56. Ranjbar-Mohammadi, M.; Nouri, M. Production and in vitro analysis of catechin incorporated electrospun gelatin/poly (lactic acid) microfibers for wound dressing applications. *J. Ind. Text.* **2022**, *51*, 7529S–7544S. [CrossRef]
57. Jiang, Z.; Li, W.J.; Wang, Y.X.; Wang, Q. Second-Order Derivation Fourier Transform Infrared Spectral Analysis of Regenerated Wool Keratin Structural Changes. *Aatcc J. Res.* **2022**, *9*, 43–48. [CrossRef]
58. Berechet, M.D.; Niculescu, M.D.; Gaidau, C.; Ignat, M.; Epure, D.G. Alkaline-Enzymatic Hydrolysis of Wool Waste for Different Applications. *Rev. Chim.* **2018**, *69*, 1649–1654. [CrossRef]
59. Leroy, M.; Labbe, J.-F.; Ouellet, M.; Jean, J.; Lefevre, T.; Laroche, G.; Auger, M.; Pouliot, R. A comparative study between human skin substitutes and normal human skin using Raman microspectroscopy. *Acta Biomater.* **2014**, *10*, 2703–2711. [CrossRef]
60. Hajikhani, M.; Emam-Djomeh, Z.; Askari, G. Fabrication and characterization of mucoadhesive bioplastic patch via coaxial polylactic acid (PLA) based electrospun nanofibers with antimicrobial and wound healing application. *Int. J. Biol. Macromol.* **2021**, *172*, 143–153. [CrossRef]
61. Berechet, M.D.; Gaidau, C.; Miletic, A.; Pilic, B.; Rapa, M.; Stanca, M.; Ditu, L.M.; Constantinescu, R.; Lazea-Stoyanova, A. Bioactive Properties of Nanofibres Based on Concentrated Collagen Hydrolysate Loaded with Thyme and Oregano Essential Oils. *Materials* **2020**, *13*, 1618. [CrossRef]
62. Roberto Medina-Medrano, J.; Alexandra Quinones-Munoz, T.; Arce-Ortiz, A.; Gabriel Torruco-Uco, J.; Hernandez-Martinez, R.; Alejandro Lizardi-Jimenez, M.; Varela-Santos, E. Antioxidant Activity of Collagen Extracts Obtained from the Skin and Gills of *Oreochromis* sp. *J. Med. Food* **2019**, *22*, 722–728. [CrossRef]
63. Kaczmarek-Szczepanska, B.; Polkowska, I.; Malek, M.; Kluczynski, J.; Pazdzior-Czapula, K.; Wekwejt, M.; Michno, A.; Ronowska, A.; Palubicka, A.; Nowicka, B.; et al. The characterization of collagen-based scaffolds modified with phenolic acids for tissue engineering application. *Sci. Rep.* **2023**, *13*, 9966. [CrossRef]
64. Kaneda, Y.; Tsutsumi, Y.; Yoshioka, Y.; Kamada, H.; Yamamoto, Y.; Kodaira, H.; Tsunoda, S.; Okamoto, T.; Mukai, Y.; Shibata, H.; et al. The use of PVP as a polymeric carrier to improve the plasma half-life of drugs. *Biomaterials* **2004**, *25*, 3259–3266. [CrossRef]
65. Su, J.; Li, J.; Liang, J.; Zhang, K.; Li, J. Hydrogel Preparation Methods and Biomaterials for Wound Dressing. *Life* **2021**, *11*, 1016. [CrossRef]
66. Nuutila, K.; Eriksson, E. Moist Wound Healing with Commonly Available Dressings. *Adv. Wound Care* **2021**, *10*, 685–698. [CrossRef] [PubMed]
67. Rapa, M.; Stefan, L.M.; Preda, P.; Darie-Nita, R.N.; Gaspar-Pintiliescu, A.; Seciu, A.M.; Vasile, C.; Matei, E.; Predescu, A.M. Effect of hydrolyzed collagen on thermal, mechanical and biological properties of poly(lactic acid) bionanocomposites. *Iran. Polym. J.* **2019**, *28*, 271–282. [CrossRef]

68. Râpă, M.; Zaharescu, T.; Stefan, L.M.; Gaidău, C.; Stănculescu, I.; Constantinescu, R.R.; Stanca, M. Bioactivity and Thermal Stability of Collagen–Chitosan Containing Lemongrass Essential Oil for Potential Medical Applications. *Polymers* **2022**, *14*, 3884. [CrossRef] [PubMed]
69. Ramirez, D.S.O.; Cruz-Maya, I.; Vineis, C.; Tonetti, C.; Varesano, A.; Guarino, V. Design of Asymmetric Nanofibers-Membranes Based on Polyvinyl Alcohol and Wool-Keratin for Wound Healing Applications. *J. Funct. Biomater.* **2021**, *12*, 76. [CrossRef]